

# Tracking *E. coli* runs and tumbles with scattering solutions and digital holographic microscopy

ANNA WANG,<sup>1</sup> REES F. GARMANN,<sup>1</sup> AND VINOOTHAN N. MANOHARAN<sup>1,2\*</sup>

<sup>1</sup>Harvard John A. Paulson School of Engineering and Applied Sciences, Harvard University, Cambridge MA 02138, USA

<sup>2</sup>Department of Physics, Harvard University, Cambridge MA 02138, USA

\*[vnm@seas.harvard.edu](mailto:vnm@seas.harvard.edu)

**Abstract:** We use in-line digital holographic microscopy to image freely swimming *E. coli*. We show that fitting a light scattering model to *E. coli* holograms can yield quantitative information about the bacterium's body rotation and tumbles, offering a precise way to track fine details of bacterial motility. We are able to extract the cell's three-dimensional (3D) position and orientation and recover behavior such as body angle rotation during runs, tumbles, and pole reversal. Our technique is label-free and capable of frame rates limited only by the camera.

© 2016 Optical Society of America

**OCIS codes:** (090.0090) Holography; (090.1995) Digital holography; (100.3190) Inverse problems; (100.3200) Inverse scattering; (170.6900) Three-dimensional microscopy; (170.3880) Medical and biological imaging.

## References and links

1. H. C. Berg and D. A. Brown, "Chemotaxis in *Escherichia coli* analysed by three-dimensional tracking," *Nature* **239**, 500–504 (1972).
2. B. Liu, M. Gulino, M. Morse, J. X. Tang, T. R. Powers, and K. S. Breuer, "Helical motion of the cell body enhances *Caulobacter crescentus* motility," *Proceedings of the National Academy of Sciences* **111**, 11252–11256 (2014).
3. K. M. Taute, S. Gude, S. J. Tans, and T. S. Shimizu, "High-throughput 3D tracking of bacteria on a standard phase contrast microscope," *Nature Communications* **6**, 8776 (2015).
4. T. Kreis, *Handbook of Holographic Interferometry* (Wiley-VCH Verlag GmbH & Co. KGaA, 2005).
5. M. Molaei, M. Barry, R. Stocker, and J. Sheng, "Failed Escape: Solid Surfaces Prevent Tumbling of *Escherichia coli*," *Physical Review Letters* **113**, 068103 (2014).
6. K. L. Thornton, R. C. Findlay, P. B. Walrad, and L. G. Wilson, "Investigating the swimming of microbial pathogens using digital holography," in "Biophysics of Infection," C. M. Leake, ed. (Springer International Publishing, Cham, 2016), pp. 17–32.
7. J. L. Nadeau, Y. B. Cho, and C. A. Lindensmith, "Use of dyes to increase phase contrast for biological holographic microscopy," *Optics Letters* **40**, 4114 (2015).
8. L. G. Wilson, L. M. Carter, and S. E. Reece, "High-speed holographic microscopy of malaria parasites reveals ambidextrous flagellar waveforms," *Proceedings of the National Academy of Sciences* **110**, 18769–18774 (2013).
9. T.-W. Su, L. Xue, and A. Ozcan, "High-throughput lensfree 3D tracking of human sperms reveals rare statistics of helical trajectories," *Proceedings of the National Academy of Sciences* **109**, 16018–16022 (2012).
10. J. F. Jikeli, L. Alvarez, B. M. Friedrich, L. G. Wilson, R. Pascal, R. Colin, M. Pichlo, A. Rennhack, C. Brenker, and U. B. Kaupp, "Sperm navigation along helical paths in 3D chemoattractant landscapes," *Nature Communications* **6**, 7985 (2015).
11. Y. Pu and H. Meng, "Intrinsic aberrations due to Mie scattering in particle holography," *Journal of the Optical Society of America A* **20**, 1920–1932 (2003).
12. F. C. Cheong, B. J. Krishnatreya, and D. G. Grier, "Strategies for three-dimensional particle tracking with holographic video microscopy," *Optics Express* **18**, 13563–13573 (2010).
13. S. Takeuchi, W. R. DiLuzio, D. B. Weibel, and G. M. Whitesides, "Controlling the shape of filamentous cells of *Escherichia coli*," *Nano Letters* **5**, 1819–1823 (2005).
14. S. Lee, Y. Roichman, G. Yi, S. Kim, Y. Seung-Man, A. van Blaaderen, P. van Oostrum, and D. G. Grier, "Characterizing and tracking single colloidal particles with video holographic microscopy," *Optics Express* **15**, 18275–18282 (2007).
15. B. Ovrn and S. H. Izen, "Imaging of transparent spheres through a planar interface using a high-numerical-aperture optical microscope," *Journal of the Optical Society of America A* **17**, 1202–1213 (2000).
16. C. Wang, X. Zhong, D. B. Ruffner, A. Stutt, L. A. Phillips, M. D. Ward, and D. G. Grier, "Holographic characterization of protein aggregates," *Journal of Pharmaceutical Sciences* **105**, 1074 – 1085 (2016).

17. C. P. Kelleher, A. Wang, G. I. Guerrero-García, A. D. Hollingsworth, R. E. Guerra, B. J. Krishnatreya, D. G. Grier, V. N. Manoharan, and P. M. Chaikin, “Charged hydrophobic colloids at an oil-aqueous phase interface,” *Phys. Rev. E* **92**, 062306 (2015).
18. J. Fung, K. E. Martin, R. W. Perry, D. M. Kaz, R. McGorty, and V. N. Manoharan, “Measuring translational, rotational, and vibrational dynamics in colloids with digital holographic microscopy,” *Optics Express* **19**, 8051–8065 (2011).
19. R. W. Perry, G. Meng, T. G. Dimiduk, J. Fung, and V. N. Manoharan, “Real-space studies of the structure and dynamics of self-assembled colloidal clusters,” *Faraday Discussions* **159**, 211–234 (2012).
20. B. Ovrn, “Three-dimensional forward scattering particle image velocimetry applied to a microscopic field-of-view,” *Experiments in Fluids* **29**, S175–S184 (2000).
21. D. M. Kaz, R. McGorty, M. Mani, M. P. Brenner, and V. N. Manoharan, “Physical ageing of the contact line on colloidal particles at liquid interfaces,” *Nature Materials* **11**, 138–142 (2012).
22. S. Wright, B. Walia, J. S. Parkinson, and S. Khan, “Differential activation of *Escherichia coli* chemoreceptors by blue-light stimuli,” *Journal of Bacteriology* **188**, 3962–3971 (2006).
23. J. Schwarz-Linek, J. Arlt, A. Jepsen, A. Dawson, T. Vissers, D. Miroli, T. Pilizota, V. A. Martinez, and W. C. Poon, “*Escherichia coli* as a model active colloid: A practical introduction,” *Colloids and Surfaces B: Biointerfaces* **137**, 2–16 (2016).
24. M. A. Yurkin and A. G. Hoekstra, “The discrete-dipole-approximation code ADDA: capabilities and known limitations,” *Journal of Quantitative Spectroscopy and Radiative Transfer* **112**, 2234–2247 (2011).
25. A. Wang, T. G. Dimiduk, J. Fung, S. Razavi, I. Kretzschmar, K. Chaudhary, and V. N. Manoharan, “Using the discrete dipole approximation and holographic microscopy to measure rotational dynamics of non-spherical colloidal particles,” *Journal of Quantitative Spectroscopy and Radiative Transfer* **146**, 499 – 509 (2014).
26. J. Saragosti, P. Silberzan, and A. Buguin, “Modeling *E.coli* Tumbles by Rotational Diffusion. Implications for Chemotaxis,” *PLoS ONE* **7**, e35412 (2012).
27. N. C. Darnton, L. Turner, S. Rojevsky, and H. C. Berg, “On torque and tumbling in swimming *Escherichia coli*,” *Journal of bacteriology* **189**, 1756–1764 (2007).
28. H. C. Berg and L. Turner, “Cells of *Escherichia coli* swim either end forward.” *Proceedings of the National Academy of Sciences* **92**, 477–479 (1995).
29. S. Bianchi, F. Saglimbeni, A. Lepore, and R. Di Leonardo, “Polar features in the flagellar propulsion of *E. coli* bacteria,” *Phys. Rev. E* **91**, 062705 (2015).
30. P. Liu, L. Chin, W. Ser, T. Ayi, P. Yap, T. Bourouina, and Y. Leprince-Wang, “Real-time measurement of single bacterium’s refractive index using optofluidic immersion refractometry,” *Procedia Engineering* **87**, 356 – 359 (2014).

## 1. Introduction

The ability to image microorganisms in motion is central to understanding how they navigate their complex physical and chemical environments. There are many studies of microbial motion in three-dimensions: the pioneering work of Berg *et al.* [1] and, more recently, Liu *et al.* [2] used microscopes with a moving stage to keep the cell in focus and centered as it swims. Taute *et al.* [3] used a diffraction-based imaging approach to track micrometer-sized bacteria with a modified phase-contrast microscope. The advantage of diffraction-based techniques—and more broadly, interferometric techniques—is that interference patterns can be captured even when the object is not in the focal plane, eliminating the need for a moving stage. The trade-off is that the patterns are more difficult to interpret than in-focus images.

A related technique, holographic microscopy, uses coherent light to illuminate the sample. The hologram that results from the interference of scattered and undiffracted light can be digitally post-processed to obtain images that resemble bright-field microscopy images. These images, called reconstructions, are obtained by numerically back-propagating light through the holograms [4]. Unlike diffraction-based techniques, holographic images preserve phase differences between different parts of the scattered field, and thus three-dimensional positions can be recovered without calibration. Time-series of reconstructions can be used to track the center-of-mass trajectories of *E. coli* [5–7], malaria gametes [8], and sperm [9, 10]. However, it is difficult to recover orientational information from reconstructions, owing to distortions in the axial direction [11, 12].

Extracting the orientation of the cell during motion is a challenge common to most imaging techniques. As a result, the orientation of the cell body is rarely tracked for the entire duration of the trajectory in microorganism motility studies. Because the cell’s hydrodynamics are important to the motion [2, 13], an understanding of microorganism motility is incomplete without knowledge

of how the cell body is oriented as a function of time.

Here we demonstrate a holographic method to quantitatively track the orientation of the model organism *Escherichia coli* as the bacteria swim in a 3D environment. Instead of doing reconstructions, we fit a light-scattering model for the cell to the holograms. Scattering solutions have proven useful for tracking and characterizing colloidal particles: they were first used to analyze holograms of colloidal spheres [14, 15], and since then have been used to characterize protein aggregates [16], indirectly measure the number of elementary charges on particles [17], study the vibrational dynamics and rearrangements of colloidal clusters [18, 19], do three-dimensional particle image velocimetry [20], and probe how particles interact with oil-water interfaces [21].

Until now, these methods have not been applied to tracking bacteria such as *E. coli*, which are optically inhomogeneous and whose shape can vary from cell to cell. Indeed, Nadeau *et al.* [7] found that it was necessary to dye the bacteria to improve the refractive index contrast enough to image them with holographic microscopy. Their method relied on reconstruction of the phase. We show that it is possible to track the orientation of unlabeled *E. coli* cells as they freely swim in 3D by fitting an electromagnetic scattering solution of a spherocylinder to the holograms of the cells. Despite the optical inhomogeneity and the deviations of the cell shape from the spherocylinder approximation, we are nonetheless able to obtain precise measurements of the orientation and position. We show that our technique yields an order-of-magnitude improvement in precision over diffraction-based techniques [3] with a much simpler apparatus than is used in moving-stage techniques. Furthermore, our technique uses monochromatic 660 nm laser light, whereas the shorter wavelengths used in fluorescence and bright field imaging can alter the motility of *E. coli* in nutrient-rich broth [22].

## 2. Materials and methods

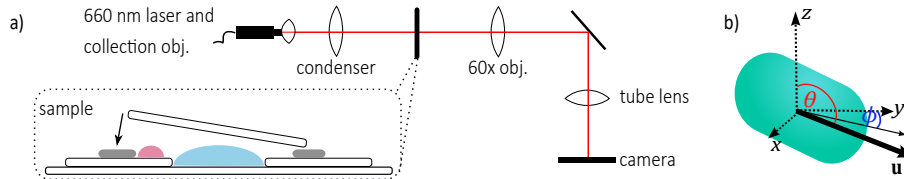


Fig. 1. a) Holograms are captured on an in-line holography setup, shown at top. Our sample cells (bottom) consist of two square coverslips glued with epoxy to a larger coverslip. A droplet of tryptone broth (blue) is placed in between the smaller coverslips. A smaller droplet of cells (pink) is placed on the smaller coverslip. A top coverslip is sealed in place with vacuum grease (gray). b) We define the orientation and position of the *E. coli* cell relative to the laboratory frame. A unit vector  $\mathbf{u}$  points along the long axis of the cell in the direction of travel. The angle between  $\mathbf{u}$  and the imaging axis ( $z$ -axis) is defined to be the polar angle  $\theta$ . We define another unit vector  $\mathbf{p}$  that is a projection of  $\mathbf{u}$  onto the  $x$ - $y$  plane. The angle that  $\mathbf{p}$  makes with the laboratory  $y$ -axis is the azimuthal angle  $\phi$ .

### 2.1. *E. coli* samples

To prepare *E. coli* samples, we first prepare the growth media for the bacteria. We make Luria broth (LB) by mixing 5 g tryptone (Difco Laboratories), 2.5 g Yeast Extract (Difco Laboratories), 2.5 g NaCl (final concentration 86 mM, Sigma-Aldrich), and enough deionized water (Elix, EMD Millipore) to make 500 mL of broth. We filter the broth through a 0.22  $\mu\text{m}$  filter (500 mL PES vacuum filter, Corning USA), and store the broth at room temperature ( $21 \pm 2^\circ\text{C}$ ). We make Tryptone broth (TB) using the LB recipe but omit the Yeast Extract.

We then follow a two-day procedure to grow motile *E. coli* from a frozen stock solution of wild-type *AW405* cells (gift from Karen Fahrner and Howard Berg). We prepare 5–10 mL of LB in a sterile culture tube (VWR International), scrape a pipette-tip against the frozen stock, and add the scraped cells to the LB solution. The inoculated LB is kept overnight at 37°C on an incubator shaker (New Brunswick Scientific, C24) that shakes at 200 rpm.

The next morning, we warm 50 mL of TB to 33°C in a small Erlenmeyer flask that has been cleaned in a pyrolysis oven (Pyro-Clean Tempyrox). We add 500  $\mu\text{L}$  of the overnight solution to the flask and incubate the flask at 33°C while shaking at 200 rpm. We check the cell density in the flask every hour on a CO8000 Cell Density Meter (WPA Biowave). Once the cell density reaches an optical density ( $\text{OD}_{600}$ ) of 0.5, we remove the flask from the incubator. We dilute the solution of cells 1:10 by volume with TB just prior to imaging.

Our sample chambers consist of a series of glass coverslips (No. 1 VWR), as shown in Fig. 1. Two  $18 \times 18$  mm coverslips are affixed to a  $24 \times 60$  mm coverslip with UV-curable epoxy (Norland 60) to create two “shelves” and a central chamber. A 100  $\mu\text{L}$  drop of tryptone broth is deposited in the central chamber. We place polydimethylsiloxane grease (Dow Corning high vacuum grease) around the chamber to form walls, then add 10  $\mu\text{L}$  of diluted *E. coli* broth onto one shelf. All pipetting of the *E. coli* is performed with a cut pipette tip to minimize shear damage to the flagella [23]. A final  $22 \times 22$  mm coverslip is placed on top of the vacuum grease to seal the chamber. *E. coli* tumble less and become easily trapped near surfaces [5], and thus we expect many cells to be trapped on the shelf on which they are first deposited. Because we are interested in cells swimming in the bulk, we image only the central chamber, which contains only those cells that have swum into the bulk from the sample we placed on the shelf.

## 2.2. Taking holograms

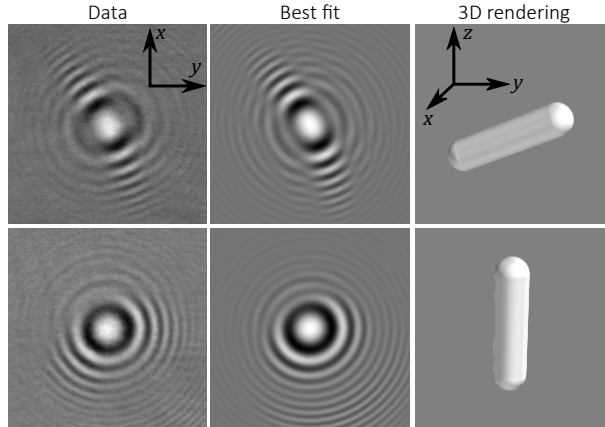


Fig. 2. We capture holograms of freely swimming *E. coli* in a time series. Two frames are shown in the left column, where the asymmetry in the fringes is noticeably different between the frames. The best-fit holograms are shown in the middle, and three-dimensional renderings from the best-fit holograms are shown on the right.

We use an in-line digital holographic microscope. Laser light ( $\lambda = 660$  nm, Opnext HL6545MG) is spatially filtered with a single mode optical fiber (OzOptics SMJ-3U3U-633-4/125-3-5). It then passes through a 10 $\times$  objective (Newport) and a condenser (LWD 0.52, Nikon) to provide even, approximately plane-wave illumination on the sample. We use a 60 $\times$ , numerical aperture (NA) = 1.2, water-immersion objective (Nikon CFI Plan Apo VC 60 $\times$  WI) to capture the interference pattern, or hologram, formed by the scattered and undiffracted beams. We capture holograms

(Fig. 2) at 100 frames per second with a Photon Focus MVD-1024E-160 camera, store them in RAM using a frame grabber (EPIX PIXCI E4), and then transfer them to disk for analysis. The exposure time is 0.05 ms. We choose this time to be short compared to the full-frame timescale (1/100 Hz = 10 ms) to minimize blurring due to bacterial motion.

### 2.3. Analyzing holograms

Because *E. coli* are small and have little refractive index contrast with water ( $n_{E.coli}=1.36-1.39$  vs  $n_{water}=1.33$ ), they are difficult to see in raw holograms [7]. To enhance contrast and to remove imaging artifacts from uneven illumination and dust in the optical train, we divide each raw hologram by a background frame taken at a region that contains no cells. Background division yields holograms with good fringe contrast, as shown in Fig. 2. We find that cells up to 60  $\mu\text{m}$  away from the focal plane have sufficient fringe contrast for us to track them. Lower NA objectives can be used to obtain larger depths of field, at the cost of lower resolution.

We then fit a discrete-dipole based light-scattering model to the recorded holograms using the software package HoloPy (<http://manoharan.seas.harvard.edu/holopy/>) and the A-DDA program [24]. In brief, we use A-DDA to generate a scattered field for a spherocylinder, numerically interfere the field with a reference field to generate a model hologram, and then vary the parameters of the model using a Levenberg-Marquardt algorithm until the sum of squared differences, calculated pixel-by-pixel, between the model and measured holograms is minimized. The adjustable parameters in the fit are the spherocylinder’s refractive index, radius, length, three-dimensional center-of-mass coordinates, and orientation relative to the lab frame (see Fig. 1b). We initialize the Levenberg-Marquardt fitting algorithm with a guess of all of these parameters. We use the fit results from one frame as the initial guess for the following frame in the time-series.

In Wang *et al.* [25], we used a similar protocol to track silica spherocylinders with sizes similar to that of *E. coli* to a precision of 35 nm in the center of mass and  $2^\circ$  in the orientation [25]. When tracking live bacteria, we expect the tracking precision to vary from cell to cell, depending on how much the cell’s shape deviates from a spherocylinder. To quantify how well the light scattering model fits our data, we compare the best-fit holograms to the data. We evaluate the coefficient of determination  $R^2 = 1 - \sum (I_{\text{data}} - I_{\text{fit}}) / \sum (I_{\text{data}} - 1)$ , where  $I$  is the background-divided and normalized hologram, and the sum is over all the pixels. A perfect fit results in  $R^2=1$ . We find that for cells that fit with  $R^2 = 0.85$ , the standard error in the fit ranges from 2–5 nm in  $x$  and  $y$ , 20–40 nm in  $z$ , and  $7-25^\circ$  for the orientation.

## 3. Results and discussions

First we demonstrate that the spherocylinder scattering model is a good approximation for the scattering from *E. coli*. Examples of best-fit holograms and three-dimensional rendering of the fits are shown in Fig. 2. When we previously fit a DDA model to holograms of silica spherocylinders in Wang *et al.* [25], we obtained  $R^2 \approx 0.9$ . Here we find  $R^2$  between 0.8 and 0.9 depending on the cell. Cells can be tracked so long as the fringe contrast is much greater than that of nearby cells. We work with a dilute system such that cells minimally interfere, both optically and hydrodynamically, with one another. In principle, a model of multiple cells can be fit to the data to analyze denser samples, but this approach is much more computationally intensive.

To determine whether this  $R^2$  value is sufficient to track motion, we examine the motion of the cells to see whether it agrees with observations from other imaging techniques. *E. coli* move by “run and tumble,” which consists of alternating straight runs in one direction, and tumbles that cause seemingly random reorientation [1, 26]. We show a run in detail in Fig. 3. This cell travels 78  $\mu\text{m}$  in 3.4 seconds (velocity = 23.3  $\mu\text{m/s}$ ). This speed is within the expected range for *AW405* (see Table 1) [27]. We define a unit vector  $\mathbf{u}$  that points along the long axis of the cell in the direction of travel (Fig. 1b). We find that  $\mathbf{u}$  rotates about the direction of the travel.

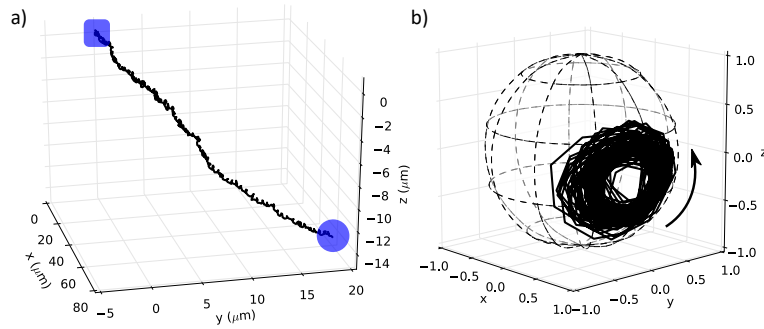


Fig. 3. a) We capture holograms of freely swimming *E. coli* in a time series and fit a scattering model to them to recover the trajectory. The blue square represents the position at the start of the time series. The circle marks the position at the end. b) We plot the direction  $\mathbf{u}$  points on a unit sphere for the duration of the trajectory in a) to show how  $\mathbf{u}$  precesses as the cell swims.

This type of rotation is known as a “wobble” [27]. We represent how  $\mathbf{u}$  changes over time on a unit sphere, as shown in Fig. 3b, and find that the wobble is  $50^\circ$ . This value is also within the expected range for *AW405* (see Table 1) [27]. For *E. coli* swimming in bulk solution, we expect the average direction of  $\mathbf{u}$  to be aligned with the direction the cell is swimming. The average direction for  $\mathbf{u}$  is  $\theta = 99^\circ$ ,  $\phi = 14^\circ$ , and the direction the cell is swimming is  $\theta = 97^\circ$ ,  $\phi = 13^\circ$ . These two values agree within the measuring precision for silica spherocylinders,  $2^\circ$  [25]. These results show that the dynamics of the cell are captured accurately.

Because we can track the body rotation of the cells, we can track the tumbling behavior. Tumbling is often modeled as rotational diffusion [26]; although this viewpoint may capture the statistics of tumbles, it neglects the mechanism by which cells actually change direction. Furthermore, diffusion cannot explain recent results from Taute *et al.*, who found that the mean change in direction after a tumble is anti-correlated with the speed of the preceding run [3].

As a first step toward elucidating the mechanics of tumbling, we track the orientation of cells as they tumble. The usual signature of a tumble is an abrupt velocity change during the trajectory. By this criterion, the bacterium shown in Fig. 4 tumbles twice, each time changing direction by approximately  $90^\circ$  (marked in red in Fig. 4a). During these events, we can track  $\mathbf{u}$  and plot its orientation on a sphere (Fig. 4b).

We see that the direction of travel changes without much body reorientation during the first tumble (Fig. 4b, left). During runs, the leading end of *E. coli* always rotates clockwise [27] when viewed from the center of the cell. This direction is dictated by the rotation of the flagellum motor and hence flagellar bundle. During this tumble event, the cell changes directions by approximately  $90^\circ$  without disrupting the clockwise precession of  $\mathbf{u}$ , indicating that the bundle is likely intact during the direction change.

The second tumble (Fig. 4b, right) is more involved. The cell appears to rotate clockwise (when viewed from the center of the sphere) before and after the tumble (black and gray lines), but counterclockwise during the tumble (red line). This apparent change in rotation from clockwise to counterclockwise could indicate that the leading end of the cell has briefly become the trailing end during the tumble. This switching of ends is also known as a pole reversal [28, 29]. This second change in direction could be interpreted either as one tumble or as two tumbles with a short-lived pole reversal in between. Either way, these trajectories demonstrate that the complexity of a tumble can vary significantly for the same change in direction.

Finally, we compare values of the parameters that we measure (Table 1) to values from the literature. We measure the refractive index, size, run speed, wobble frequency, and wobble angle

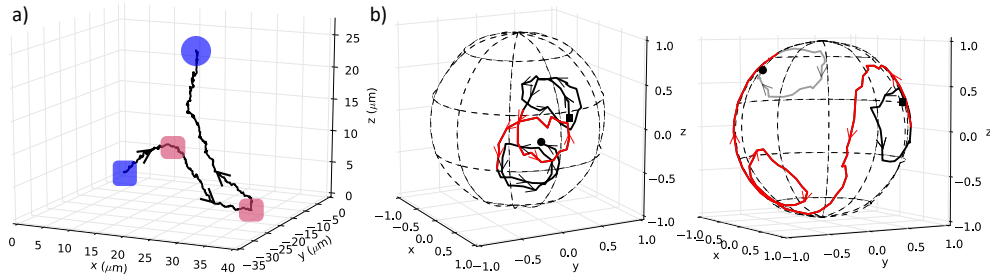


Fig. 4. a) Center-of-mass trajectory of a cell's runs and tumbles. The blue square represents the position at the start of the time series. The circle marks the position at the end. The red squares mark the two tumbles shown in panel (b). b) We plot where  $\mathbf{u}$  points on a sphere and indicate the tumbles in red. The gray part of the trajectory on the right, near the end, lies on the rear hemisphere. The square represents the start of the trajectory, the circle marks the end, and the arrows indicate the direction of motion.

for the cells, and we find that the agreement is good for all of these values, further validating our technique.

Table 1. Properties of *AW405* cells determined from fitting holograms of ten cells, compared to values from Darnton *et al.* [27] unless otherwise specified. The errors are standard deviations from the mean of measurements of ten different cells.

|            | Length ( $\mu\text{m}$ ) | Width ( $\mu\text{m}$ ) | $n$                    | Run speed ( $\mu\text{m/s}$ ) | Wobble freq. (Hz) | Wobble angle ( $^\circ$ ) |
|------------|--------------------------|-------------------------|------------------------|-------------------------------|-------------------|---------------------------|
| Our values | $2.4 \pm 0.6$            | $0.95 \pm 0.06$         | $1.41 \pm 0.01$        | $25 \pm 5$                    | $26 \pm 9$        | $68 \pm 42$               |
| Other work | $2.5 \pm 0.6$            | $0.88 \pm 0.09$         | $1.388 \pm 0.005$ [30] | $25 \pm 8$                    | $24 \pm 12$       | $46 \pm 24$               |

## 4. Conclusion

We have shown that by fitting a light scattering model to digital holograms, we can quantitatively track the 3D orientation and motion of freely swimming *E. coli*. We can track the cells with sufficient temporal resolution and spatial precision to resolve their wobbles and tumbles. The spatial precision is improved by an order of magnitude relative to other holographic [5] and diffraction-based [3] techniques.

Also, unlike other techniques for tracking microorganisms, our technique does not require a moving stage, and we are able to track the orientation of the cells for the entire trajectory. This technique can be used for studying bacteria as they freely traverse chemical and physical landscapes, providing insights into how runs and tumbles are altered by the environment. In particular, resolving the orientation of the cell body during tumbles may provide valuable constraints for models of the mechanics of the flagella during tumbles. Acquiring more data with this method might also help improve models for the hydrodynamics of runs and tumbles.

## Funding

National Science Foundation (NSF) (DMR-1306410, DMR-1420570); Army Research Office MURI (W911NF-13-1-0383).

## Acknowledgments

We thank Karen Fahrner and Howard Berg for the *AW405* cells and their growth protocol.